ACCOUNTS
of chemical research

Reversible, Long-Range Radical Transfer in *E. coli* Class Ia Ribonucleotide Reductase

ELLEN C. MINNIHAN,[†] DANIEL G. NOCERA,[*,§] AND JOANNE STUBBE[*,†,‡]

[†]*Department of Chemistry and* [‡]*Department of Biology, Massachusetts Institute of Technology, 77 Massachusetts Avenue, Cambridge, Massachusetts 02139, United States, and* [§]*Department of Chemistry and Chemical Biology, Harvard University, 12 Oxford Street, Cambridge, Massachusetts 02138, United States*

RECEIVED ON FEBRUARY 6, 2013

CONSPECTUS

Ribonucleotide reductases (RNRs) catalyze the conversion of nucleotides to 2′-deoxynucleotides and are classified on the basis of the metallo-cofactor used to conduct this chemistry. The class Ia RNRs initiate nucleotide reduction when a stable diferric-tyrosyl radical (Y•, $t_{1/2}$ of 4 days at 4 °C) cofactor in the β2 subunit transiently oxidizes a cysteine to a thiyl radical (S•) in the active site of the α2 subunit. In the active $\alpha2\beta2$ complex of the class Ia RNR from *E. coli*, researchers have proposed that radical hopping occurs reversibly over 35 Å along a specific pathway comprised of redox-active aromatic amino acids: Y_{122}• ↔ [W_{48}?] ↔ Y_{356} in β2 to Y_{731} ↔ Y_{730} ↔ C_{439} in α2. Each step necessitates a proton-coupled electron transfer (PCET). Protein conformational changes constitute the rate-limiting step in the overall catalytic scheme and kinetically mask the detailed chemistry of the PCET steps. Technology has evolved to allow the site-selective replacement of the four pathway tyrosines with unnatural tyrosine analogues. Rapid kinetic techniques combined with multifrequency electron paramagnetic resonance, pulsed electron–electron double resonance, and electron nuclear double resonance spectroscopies have facilitated the analysis of stable and transient radical intermediates in these mutants. These studies are beginning to reveal the mechanistic underpinnings of the radical transfer (RT) process.

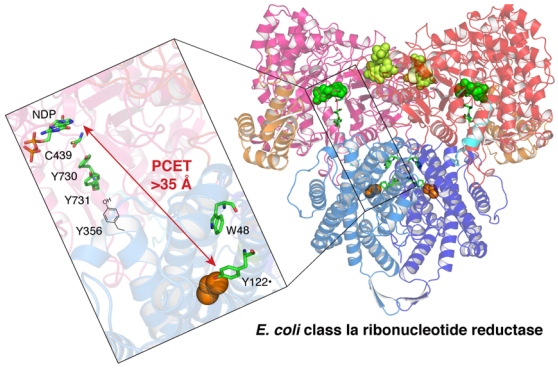

E. coli class Ia ribonucleotide reductase

This Account summarizes recent mechanistic studies on mutant *E. coli* RNRs containing the following tyrosine analogues: 3,4-dihydroxyphenylalanine (DOPA) or 3-aminotyrosine (NH_2Y), both thermodynamic radical traps; 3-nitrotyrosine (NO_2Y), a thermodynamic barrier and probe of local environmental perturbations to the phenolic pK_a; and fluorotyrosines (F_nYs, $n = 2$ or 3), dual reporters on local pK_as and reduction potentials. These studies have established the existence of a specific pathway spanning 35 Å within a globular $\alpha2\beta2$ complex that involves one stable (position 122) and three transient (positions 356, 730, and 731) Y•s. Our results also support that RT occurs by an orthogonal PCET mechanism within β2, with Y_{122}• reduction accompanied by proton transfer from an Fe1-bound water in the diferric cluster and Y_{356} oxidation coupled to an off-pathway proton transfer likely involving E_{350}. In α2, RT likely occurs by a co-linear PCET mechanism, based on studies of light-initiated radical propagation from photopeptides that mimic the β2 subunit to the intact α2 subunit and on [^{2}H]-ENDOR spectroscopic analysis of the hydrogen-bonding environment surrounding a stabilized NH_2Y• formed at position 730. Additionally, studies on the thermodynamics of the RT pathway reveal that the relative reduction potentials decrease according to $Y_{122} < Y_{356} < Y_{731} \approx Y_{730} \leq C_{439}$, and that the pathway in the forward direction is thermodynamically unfavorable. C_{439} oxidation is likely driven by rapid, irreversible loss of water during the nucleotide reduction process. Kinetic studies of radical intermediates reveal that RT is gated by conformational changes that occur on the order of >100 s^{-1} in addition to the changes that are rate-limiting in the wild-type enzyme (~10 s^{-1}). The rate constant of one of the PCET steps is ~10^5 s^{-1}, as measured in photoinitiated experiments.

Published on the Web 06/04/2013 www.pubs.acs.org/accounts
10.1021/ar4000407

Introduction

Ribonucleotide reductases (RNRs) catalyze the conversion of nucleotides (NDPs or NTPs where N = C, U, G, or A) to 2′-deoxynucleotides (dNDPs or dNTPs)[1] and are responsible for controlling the relative ratios and absolute concentrations of cellular dNTP pools. For this reason, RNRs play a major role in ensuring the fidelity of DNA replication and repair. RNRs are found in all organisms and are classified based on the metallo-cofactor used to initiate catalysis,[1] with the class Ia RNRs requiring a diferric-tyrosyl radical (Y•) cofactor.

The prototypical class Ia RNR from *E. coli*, the subject of this Account, is composed of two subunits, $\alpha 2$ and $\beta 2$, and is active as an $\alpha 2\beta 2$ complex, as highlighted in Figure 1. $\alpha 2$ houses the catalytic site for substrate (S) reduction and two allosteric effector (E = ATP, dGTP, TTP, and dATP) binding sites that govern which S is reduced (specificity site) and the overall rate of reduction (activity site).[2] $\beta 2$ contains the essential diferric-Y• cofactor. This unusually stable Y•, located at position 122, has a $t_{1/2}$ of 4 days at 4 °C in contrast to the microsecond lifetimes observed for Y•s in solution. Nucleotide reduction occurs by a complex mechanism involving protein- and substrate-derived radicals, some details of which are summarized in Figure 2.[1,3] The stable Y_{122}• transiently oxidizes a cysteine (C_{439}) in the catalytic site to a thiyl radical (S•), which reversibly abstracts a 3′-hydrogen atom (H•) from the NDP. The 3′-nucleotide radical rapidly loses water in the first irreversible step.[1,3] The reducing equivalents are provided by two local cysteines (C_{225} and C_{462}), and the resulting disulfide is re-reduced for subsequent turnovers, ultimately by thioredoxin (TR), thioredoxin reductase (TRR), and NADPH.

Uhlin and Eklund proposed a structure of the active $\alpha 2\beta 2$ complex by in silico docking of crystal structures of the individual subunits (Figure 1).[2] An atomic-resolution structure of an active class I RNR is still not available; however, recent experimental evidence supports this model (vide infra). The interaction between subunits is governed primarily by the flexible C-terminus of $\beta 2$ (residues 360−375, Figure 1).[4] The most provocative feature of the docking model was the >35 Å distance between Y_{122}• in $\beta 2$ and C_{439} in $\alpha 2$. The long distance suggested that direct oxidation of C_{439} by Y_{122}• by a single-step, electron tunneling mechanism would be too slow (k_{ET} of 10^{-7}−10^{-9} s^{-1}) to account for the turnover number of the *E. coli* RNR (~10 s^{-1}).[5] Accordingly, Uhlin and Eklund proposed that oxidation occurred by a hopping mechanism utilizing a specific pathway of conserved aromatic amino acids: Y_{122}• ↔ [W_{48}?] ↔ Y_{356} in $\beta 2$ to Y_{731} ↔ Y_{730} ↔ C_{439} in $\alpha 2$. The necessity of these residues for catalysis was established by site-directed mutagenesis experiments.[6,7]

The thermodynamics of Y or W oxidation require that proton transfer (PT) accompanies electron transfer (ET) at physiological pH. In RNR, these transfers are proposed to occur in a concerted fashion to prevent formation of high-energy, charged intermediates, thereby requiring a proton-coupled electron transfer (PCET) at each step.[8−11] In our model, orthogonal PCET steps are operative in $\beta 2$, with the proton and electron transferring from the same donor to different acceptors, whereas co-linear PCET steps are operative in $\alpha 2$, with the proton and electron moving between the same donor/acceptor pair (Figure 3a).[7,10,11] Our current model for the thermodynamics of radical transfer (RT) has evolved from studies in which the reduction potentials have been modulated at each Y on the pathway (Figure 3b).[12−14] It holds that the potentials increase from $Y_{122} < Y_{356} < Y_{731} \approx Y_{730} \leq C_{439}$, with the uphill forward oxidation driven by irreversible loss of H_2O during nucleotide reduction. We now give an account of the results that have given rise to our RT mechanism and thermodynamic model.

Tools

Protein Engineering. The study of RT is complicated by the fact that the PCET events are masked in the wild-type (wt) RNR by rate-limiting protein conformational changes that occur upon binding of nucleotides to $\alpha 2\beta 2$ prior to RT.[5] To perturb the native RT pathway in a predictable way, we have utilized two methods for site-specific incorporation of eight unnatural amino acids (UAAs) with altered reduction potentials and/or pK_as into RNR (Figure 4a, Table 1). One method involved the semisynthesis of $\beta 2$ by expressed protein ligation (EPL),[15,16] whereas the second utilized in vivo nonsense codon suppression.[13,17] Current research focuses on the latter method, as it may be applied to any residue in either subunit, minimizes mutations to the native enzyme relative to EPL, and has allowed isolation of 100 mg quantities of protein (Figure 4b).

Kinetic Techniques and Spectroscopic Methods. The reactivity of a mutant protein, once isolated, is studied by rapid kinetic techniques to unveil radical intermediates. In a typical experiment, a solution containing a mutant subunit ($\alpha 2$ or $\beta 2$) and S is rapidly mixed with a solution containing the complementary wt subunit and E, and the reaction monitored with millisecond time resolution for loss of Y_{122}• and formation of a new radical(s) (Figure 5). Changes can be monitored continuously by stopped-flow (SF) UV−vis or fluorescence spectroscopies, or discontinuously using

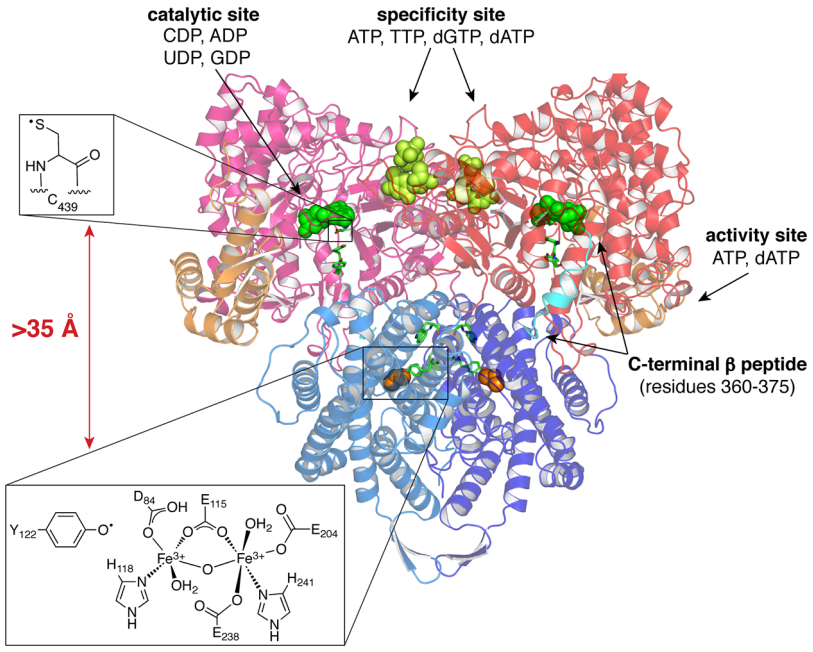

FIGURE 1. Docking model of the *E. coli* $\alpha 2\beta 2$ complex.[2] $\alpha 2$ (pink and red) contains three nucleotide binding sites. $\beta 2$ (light and dark blue) contains the diferric-Y• cofactor; residues 340−375 are not resolved in this structure. A peptide corresponding to the C-terminal 20 amino acids of β is bound to each α, a portion of which (residues 360−375) is resolved in the crystal structure (cyan). The "ATP cone" region of α, which contains the effector site that governs activity, is colored orange. This model separates Y_{122}• in $\beta 2$ from C_{439} in $\alpha 2$ by >35 Å. GDP (green), TTP (yellow), and the Fe_2O core of the diferric cluster (orange) are shown in CPK space-filling models. Residues constituting the RT pathway (green) are shown in sticks.

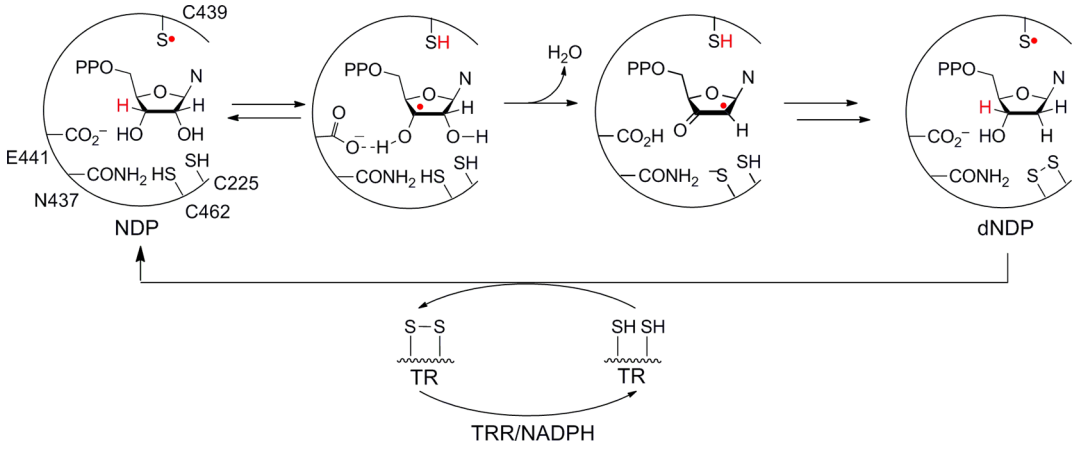

FIGURE 2. Mechanism of NDP reduction by RNR. The S• shown on C_{439} of $\alpha 2$ in the first reaction step is reversibly generated by Y_{122}• in $\beta 2$ by the mechanism shown in Figure 3a.

either a rapid freeze quench (RFQ) apparatus and paramagnetic resonance spectroscopy or a rapid chemical quench (RCQ) apparatus and scintillation counting of a radiolabeled product.

Figure 6 shows the spectroscopic signatures of the stable diferric-Y_{122}• in $\beta 2$. The cofactor gives rise to a UV−vis spectrum with a sharp feature at 411 nm (Figure 6a) and an EPR spectrum (9 GHz) with hyperfine couplings associated with one of its two β-methylene protons and its 3,5 aromatic protons (Figure 6b). The g tensors (g_x, g_y, g_z) determined by high-field (HF) EPR (94 or 140 GHz) are particularly informative, as g_x is very sensitive to the electrostatic (i.e., H-bonding) environment of the Y• (Figure 6c). EPR and related methods, including pulsed electron−electron double resonance (PELDOR)[20] and HF [^{2}H]-electron nuclear double resonance (ENDOR)[21] spectroscopies, have allowed characterization of stable and transient radicals observed in engineered RNRs. Together, these methods have provided tools for the study of RT in RNR.

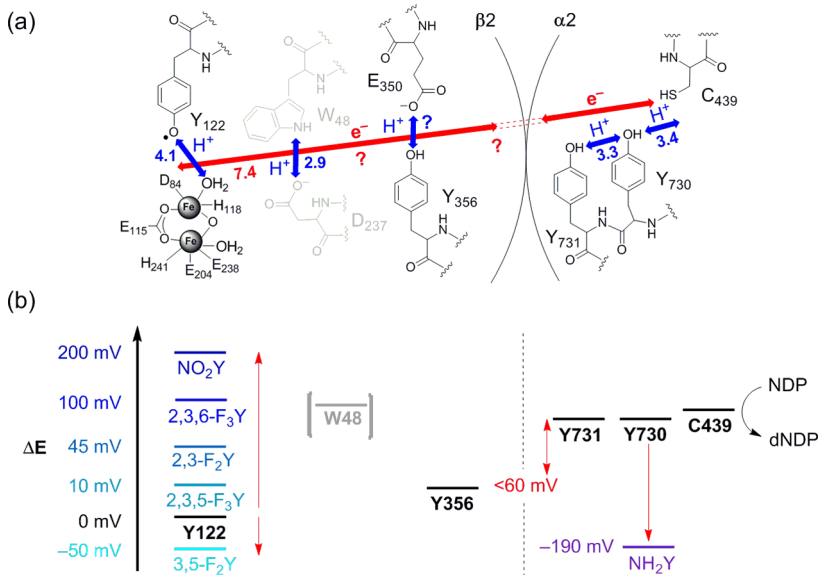

FIGURE 3. Nocera/Stubbe elaboration of the Uhlin/Eklund model for RT in *E. coli* class Ia RNR. (a) The proposed movement of protons (blue arrows) and electrons (red arrows) at each step on the pathway. Distances (Å) are from structures of α2 and β2. E_{350} and Y_{356} are disordered in all β2 structures, and their positions are unknown. There is no direct evidence that W_{48} and D_{237} participate in RT, and thus, they are shown in gray. The distance between W_{48} and Y_{731} is modeled to be 25 Å. Adapted with permission from ref 13. Copyright 2011 American Chemical Society. (b) The proposed relative reduction potentials of residues on the RT pathway from experiments using the indicated UAAs site-specifically incorporated in place of each Y. NH_2Y has been incorporated at position 356, 730, or 731. Note that the absolute reduction potentials of these residues, the structures of which are shown in Figure 4, are not known, and the relative reduction potentials indicated are our best estimates given current knowledge (see Table 1 and Footnote 1).

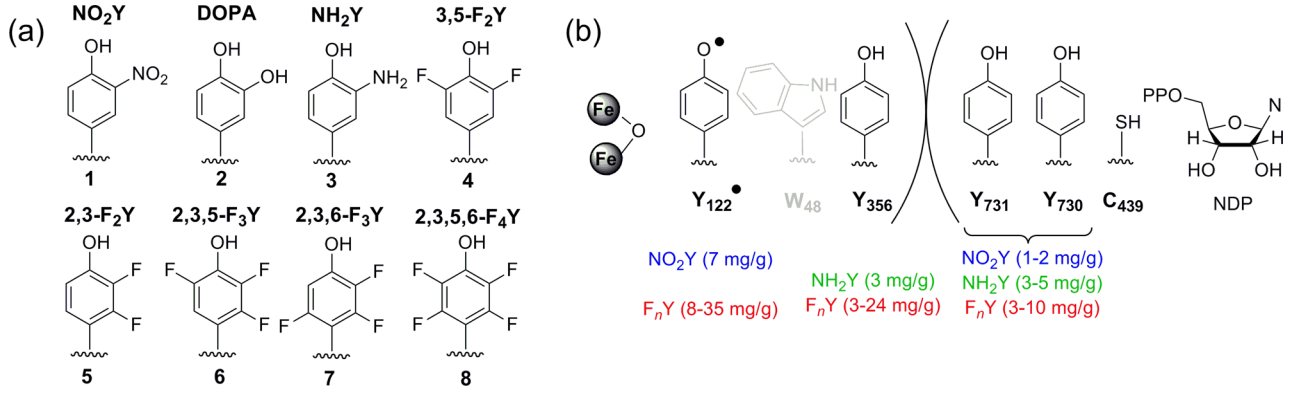

FIGURE 4. UAAs incorporated into *E. coli* class Ia RNR. (a) Compounds **1**, **2**, and **4**–**8** have been incorporated in position 356 of β2 by EPL, while compounds **1** and **3**–**7** have been incorporated to sites in both α2 and β2 by in vivo nonsense suppression. (b) Purified protein yields achieved by in vivo nonsense suppression are given in parentheses for each UAA at each position (in mg protein/g cells).

Complexities in Studying *E. coli* Class Ia RNR. Two unresolved issues have complicated our mechanistic studies. The first is the apparent half-sites reactivity of RNR,[5,19] a phenomenon in which radical initiation occurs initially within a single α/β pair and a chemical or conformational step during or subsequent to product formation then triggers RT on the second α/β pair.[5] The second RT event is prevented when a radical is trapped in the first α/β pair by replacing the S with a mechanism-based inhibitor[20] or by modulating the energetics of RT using UAAs.[19,23] The second issue concerns the stoichiometry and distribution of Y_{122}• within β2. The diferric-Y• in β2 is self-assembled from apo-β2 to give ~1.2 Y•/β2 and while the loading of radical in each β monomer is unknown, our in vitro biochemical studies suggest it is evenly distributed (0.6 Y•/β).

Evidence for a Pathway of Redox-Active Amino Acids

Our earliest experiments sought to validate the proposed pathway and the redox reactivity of its constituents (Figure 3a). The role of Y_{356} in the C-terminal tail of β2 was first studied, as its position relative to other residues is

unknown (Figure 1). Using EPL, Y_{356} was replaced with 3,4-dihydroxyphenylalanine (DOPA, **2**, Figure 4a), which has a peak potential (E_p) 260 mV lower than that of Y (pH 7, Table 1) and was utilized as a radical trap. Reaction of Y_{356}DOPA-β2 with wt-α2, S, and E resulted in loss of 50% of the initial Y_{122}• concomitant with formation of an equal amount of $DOPA_{356}$•.[19] No $DOPA_{356}$• was observed in the absence of the second subunit or nucleotides. The kinetics of $DOPA_{356}$• formation involved multiple phases, the majority of which were kinetically competent (i.e., faster than the wt k_{cat}); however, the mutant was unable to make dNDP. These studies demonstrated that nucleotides are required to trigger RT and provided the first evidence for conformational changes associated with RT.

Our attention turned to investigating the roles of Y_{731} and Y_{730} in α2. In collaboration with the Schultz lab, an orthogonal tRNA synthetase (RS) that specifically recognizes 3-aminotyrosine (NH_2Y, **3**, Figure 4a) was evolved and was used to incorporate NH_2Y to positions 730 and 731 of α2 and 356 of β2 (collectively called NH_2Y-RNRs). With an E_p 190 mV lower than that of Y (pH 7, Table 1), NH_2Y was expected to behave like DOPA, as a radical sink. Indeed, reaction of each of the three NH_2Y-RNRs with the second subunit, S, and E resulted in the generation of an NH_2Y• kinetically coupled to Y_{122}• loss, as measured by SF UV−vis and EPR spectroscopy (Figure 7).[17,24] Radical formation again required the presence of both subunits and nucleotides, was biphasic, and was kinetically competent for all S and E pairs for all three NH_2Y-RNRs. In contrast to DOPA, however, all NH_2Y-RNRs were active in dNDP production. Additional experiments revealed that NH_2Y• was formed only when the other Ys in the wt RT pathway were intact. This result was interpreted as evidence that NH_2Y• formation is pathway-dependent and not the indirect consequence of introducing a thermodynamic trap into the protein.[25] Thus, results obtained with DOPA- and NH_2Y-RNRs support the participation of three Ys acting as redox relays linking Y_{122}• in β2 to C_{439} in α2.

TABLE 1. pK_as and E_ps of UAAs

UAA[a]	pK_a[b]	E_p vs NHE (V)[c]	ΔE_p vs Y/Y• (mV)[c]
Y	9.9	0.83	
DOPA	9.7	0.57	−260
NH_2Y	∼10	0.64	−190
3,5-F_2Y	7.2	0.77	−60
2,3-F_2Y	7.8	0.86	+30
2,3,5-F_3Y	6.4	0.86	+30
2,3,6-F_3Y	7.0	0.93	+100
2,3,5,6-F_4Y	5.6	0.97	+140
NO_2Y	7.2	1.02	+190

[a]For Y, NO_2Y, and F_nYs, measurements made on *N*-acetyltyrosinamide forms. [b]The solution pK_as reported here are perturbed by <+1 unit at positions 356, 730, and 731 and by >+2.5 units at position 122. [c]At pH 7, as reported in refs 15, 17−19, and references therein.

Evidence for an Active $\alpha 2\beta 2$ Complex Resembling the Docking Model

The ability to generate moderately stabilized NH_2Y•s ($t_{1/2}$ on min scale) at positions along the pathway coupled with the half-sites reactivity of RNR allowed us to test whether the docking model (Figure 1)[2] is an accurate representation of the active RNR. Specifically, PELDOR spectroscopy, a technique that detects weak dipolar interactions between paramagnetic species separated by 20−80 Å, was utilized to measure diagonal distances between a radical generated on the pathway in one α/β pair and the Y_{122}• on the second α/β pair (Figure 8). The distances measured between Y_{122}• and $DOPA_{356}$• provided the first structural constraint on the

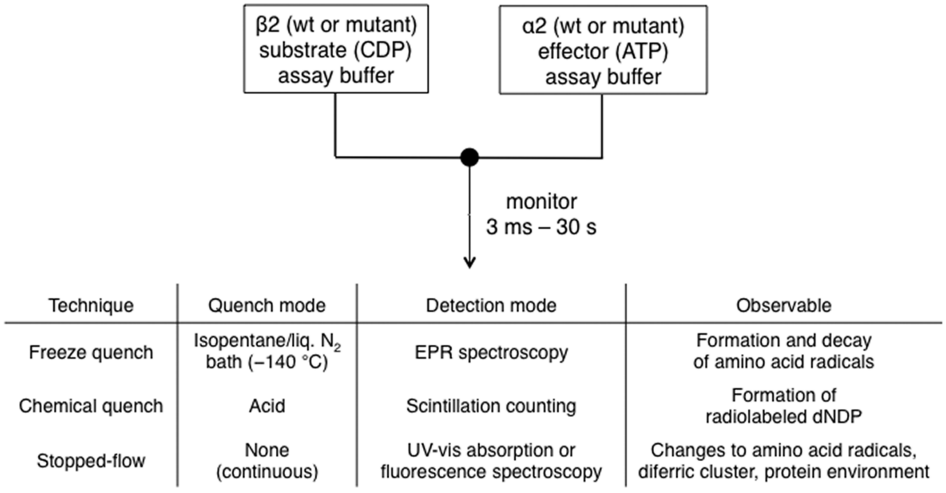

FIGURE 5. Experimental design, kinetic techniques, and detection methods for studying RT.

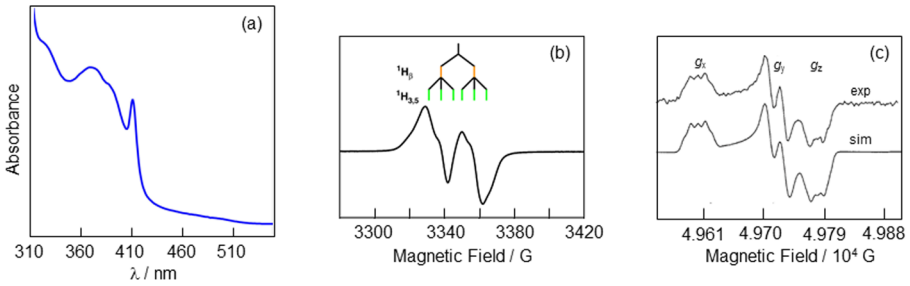

FIGURE 6. Spectroscopic characterization of the diferric-Y_{122}• cofactor from *E. coli* class Ia RNR. (a) The UV−vis spectrum has contributions from the diferric cluster at 325 and 365 nm and Y_{122}• at 411 nm. (b) The 9 GHz EPR spectrum of Y_{122}• with the origin of its hyperfine couplings indicated. (c) The 140 GHz EPR spectrum of Y_{122}• resolves three distinct *g* tensors. Panel (c) adapted with permission from ref 22. Copyright 1993 American Chemical Society.

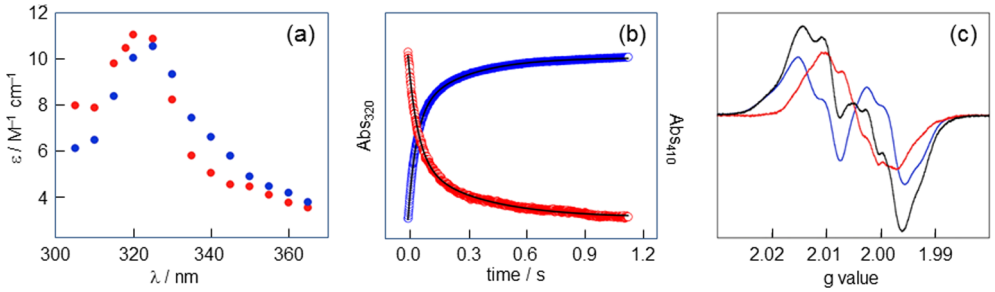

FIGURE 7. Spectroscopic characterization of NH_2Y•s. (a) A point-by-point reconstruction of the absorbance spectra of NH_2Y_{730}• (blue) and NH_2Y_{731}• (red) formed 1.5 s after reacting $Y_{731}NH_2Y$-α2 (or $Y_{730}NH_2Y$-α2) with wt-β2, CDP, and ATP. (b) Averaged single-wavelength SF UV−vis traces for the $Y_{731}NH_2Y$-α2 reaction described in (a). Loss of Y_{122}• (red, 410 nm) correlates with the formation of NH_2Y_{731}• (blue, 320 nm). Biexponential fits to the data are shown as black lines. (c) The 9 GHz EPR spectrum (black) of an identical reaction frozen after 10 s is a ~1:1 composite of residual Y_{122}• (blue) and NH_2Y_{731}• (red). Figure adapted with permission from ref 17. Copyright 2007 American Chemical Society.

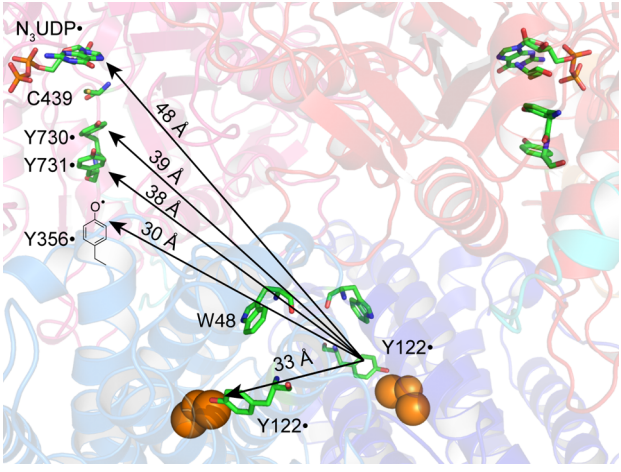

FIGURE 8. Validating the docking model by PELDOR spectroscopy. By exploiting the half-sites reactivity of RNR, diagonal distances between Y_{122}• on one α/β pair and $DOPA_{356}$•, NH_2Y_{731}•, NH_2Y_{730}•, and an active-site N• on the second α/β pair have been measured.[20,23] The pathway residues and S were built in from the docking model,[2] in which Y_{356} is invisible.

location of this residue within α2β2. Measurements between Y_{122}• and NH_2Y_{731}•, NH_2Y_{730}•, or an active-site nitrogen-centered radical formed upon reaction with the mechanism-based inhibitor 2′-azido-2′-deoxyuridine 5′-diphosphate (N_3UDP)[1] were all in excellent agreement with the distances predicted by the docking model.[20,23]

We have also observed that generation of an NH_2Y• on the pathway induces a tight, kinetically stable α2/β2 interaction.[26] At low α2 and β2 concentrations in the presence of S and E pairs, the wt α2/β2 interaction is weak (K_d = 50−400 nM) and transient (k_{off} ~ 50−100 s^{-1}).[4,27] In contrast, under conditions that generate NH_2Y_{730}•, the binding between $Y_{730}NH_2Y$-α2 and wt-β2 is tight (K_d = 7 nM), cooperative, and long-lived (k_{off} ~10^{-3} s^{-1}). The stable complex has been structurally characterized by electron microscopy (30 Å resolution) and was found to be consistent with the docking model, providing the first direct visualization of RNR in a catalytically relevant state.[26]

Mechanism of Long-Range PCET in *E. coli* RNR

pK_as of Pathway Residues. UAAs with perturbed pK_as (Figure 4a, **1** and **4**−**8**, and Table 1) provide a means to study the nature of the PT coupled to ET (i.e., orthogonal vs co-linear PCET, Figure 3a). To interpret the results of such experiments, we initially determined the extent to which the

pK_as of the pathway Ys are modulated by their local protein environment using NO_2Y (Figure 4a, **1**). The absorbance features of the NO_2Y phenolate (NO_2Y^-, λ_{max} = 430 nm, ε = 4200 cm^{-1} M^{-1}) allowed titration of a single residue in the 258 kDa complex of $\alpha2\beta2$, S and E. When incorporated at position 356 of $\beta2$ and 730 and 731 of $\alpha2$, the pK_a of NO_2Y was increased by $\leq$1 pH unit compared that of NO_2Y in solution (7.2).[15,28] In contrast, NO_2Y incorporated at position 122 of $\beta2$ revealed an increase in pK_a by >2.5 units,[28] suggesting that the hydrophobic pocket surrounding the cofactor confers unique properties on Y_{122} relative to the other pathway Ys. X-ray structures of $\alpha2$ and $\beta2$ mutants containing NO_2Y revealed minimal changes in comparison to structures of the respective wt subunits.[28,29]

Mechanism of RT in $\beta2$. Our proposal for orthogonal PCET in $\beta2$ (Figure 3a) was first examined by replacing Y_{356} with 2,3-F_2Y (**5**, Figure 4a), which has a pK_a of 7.8.[30] A pH rate profile of dCDP formation with $Y_{356}(2,3)F_2Y$-$\beta2$ and wt-$\alpha2$ revealed that the complex was active from pH 6 to 9, indicating that ET through position 356 does not require PT and suggesting that an H-bond to Y_{356} is not necessary for RT through that position.[30] Subsequently, a complete series of F_nYs (**4**–**8**, Figure 4a) with pK_as ranging from 5.6–7.8 (Table 1) were incorporated at position 356. In no case was a correlation between enzyme activity and protonation state observed, consistent with an orthogonal PCET mechanism.[16]

An orthogonal PCET mechanism involving 356 suggests the importance of a proton acceptor. This was proposed to be the conserved acid E_{350} in the C-terminus of $\beta2$ (Figure 3a) after Sjöberg and colleagues observed that E_{350}A-$\beta2$ is catalytically inactive despite maintaining its ability to bind $\alpha2$ and to assemble cofactor.[6] Furthermore, reactions between E_{350}A/$Y_{356}NH_2Y$-$\beta2$ and wt-$\alpha2$, or E_{350}A-$\beta2$ and $Y_{731}NH_2Y$-$\alpha2$, fail to generate NH_2Y•, indicating that the E_{350} mutation prevents NH_2Y oxidation at positions 356 and 731.[14] While these results highlight the importance of E_{350} in mediating RT through position 356, the inactivity of these and the E_{350}D- and E_{350}Q-$\beta2$ mutants prevents drawing strong mechanistic conclusions.

Mechanistic insight into the first step of RT, reduction of Y_{122}•, has been investigated in collaboration with the Bollinger/Krebs lab.[31] The model (Figure 3a) proposes that Y_{122}• reduction is coupled to PT from a Fe1-bound water. To test this hypothesis, the Mössbauer spectrum of the resting diferric-Y_{122}• in [^{57}Fe]-loaded wt-$\beta2$, wt-$\alpha2$, and E was compared to that of the Y•-reduced cofactor generated upon reaction of $\beta2$, $\alpha2$, and E with 2′-N_3UDP.[1] The similarities in the isomer shifts and the differences in the quadrupole splitting parameter associated with Fe1 suggest no change in the Fe oxidation state and a change in ligation to Fe1 from a bound water to a bound hydroxide, consistent with PT from this ligand to the reduced Y_{122}.[31]

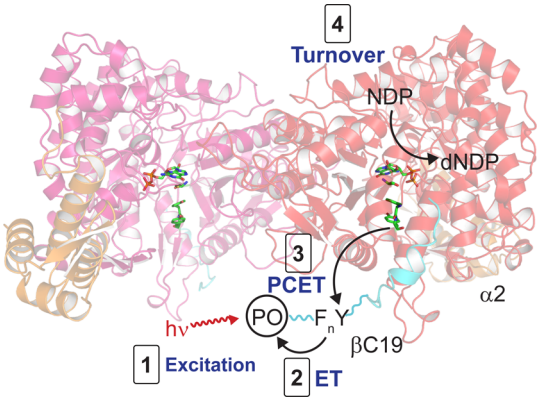

FIGURE 9. Photoinitiated radical propagation in PO-Y-βC19 photopeptides. A photooxidant (PO, black circle) is appended to the N-terminus of a peptide corresponding to residues 356–375 of $\beta2$ (βC19, cyan), with either Y or F_nY at position 356. Light excitation (step **1**) induces oxidation of the residue at position 356 (**2**), a fraction of which is reduced by Y_{731} of $\alpha2$ (**3**). The photopeptide/wt-$\alpha2$ complex is capable of generating dNDP (**4**), providing direct evidence for radical injection from the peptide. Figure constructed from PDB ID 1RLR.[2]

Mechanism of RT in $\alpha2$. Experimental evidence for co-linear PCET within $\alpha2$, suggested by the proximity of pathway residues in the $\alpha2$ structure, was obtained by studying light-initiated RT in systems in which the $\beta2$ subunit is replaced by a photopeptide (Figure 9).[7,10] The peptide corresponds to the C-terminal 19 amino acids (356–375) of β (βC19) with either a Y or F_nY at position 356 and a photooxidant (PO) such as benzophenone (BP), anthraquinone (Anq), or Re(bpy)(CO)$_3$CN ([Re]) appended to the N-terminus.[10,11] Pairing different POs with different Y analogues allows modulation of the driving force of oxidation at position 356 and of radical injection into $\alpha2$. Upon excitation, the PO generates a transient radical at 356, a small fraction of which migrates into $\alpha2$ (Figure 9). The time-resolved formation and decay of the 356 radical is monitored by transient absorption spectroscopy.

Photolysis of either [BP]- or [Anq]-Y-βC19 with wt-$\alpha2$, [^{14}C]-CDP, and ATP under single-turnover conditions generated 0.25 dCDP/$\alpha2$, demonstrating the chemical competence of the system.[32] The redox-inert Y_{730}F-$\alpha2$ prevented dCDP formation, supporting co-linear transport of an H^+ and e^-.[32] The light-initiated reaction of [Re]-2,3,6-F_3Y-βC19 with wt-$\alpha2$ was compared to that with various $\alpha2$ mutants to investigate whether the photogenerated F_3Y_{356}• could initiate RT into $\alpha2$. Radical injection occurred with a k_{et} of $\sim10^5$ s^{-1} in both the wt enzyme and C_{439}S mutant, but was not observed in the Y_{731}F and Y_{730}F variants.

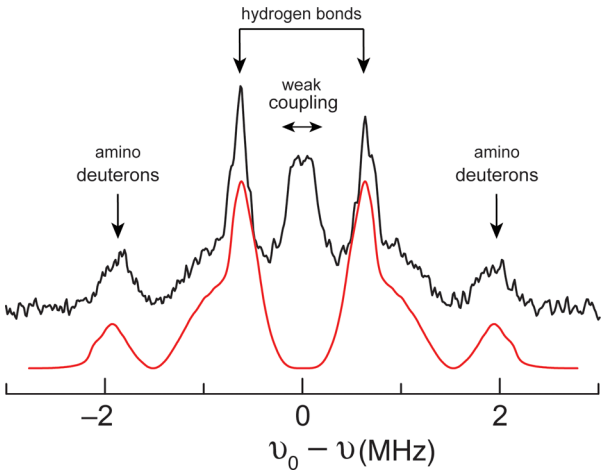

FIGURE 10. The 94 GHz [^{2}H]-MIMS ENDOR spectrum of NH_2Y_{730}• in the active $\alpha 2\beta 2$ complex reveals the details of its intra- and intermolecular H-bonds. Experimental data are shown in black and a simulation in red. The two prominent peaks centered around 0.6 MHz fall in a region expected for coupled H bonds. The detailed analysis of the experimental spectrum and its simulation is described in ref 21. Adapted with permission from ref 21. Copyright 2012 American Chemical Society.

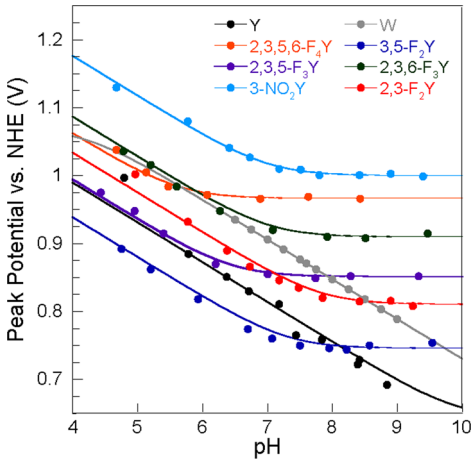

FIGURE 11. Solution peak potentials (E_ps) of Y, W, and UAAs blocked with N-acetyl and C-amide functionalities. Adapted (in part) with permission from refs 15 and 18. Copyright 2003 and 2006 American Chemical Society.

These results suggest that the intact Y_{731}/Y_{730} dyad and its associated H-bonding network are necessary for RT.[33] Experiments are underway to test this hypothesis with [Re]-C_{355}S-β2, a mutant β2 in which the PO is attached at position 355, in the intact $\alpha 2\beta 2$ complex.[34]

Additional support for co-linear PCET within α2 has been obtained from studies of the NH_2Y_{730}• formed upon reaction of $Y_{730}NH_2Y$-α2 with wt-β2, CDP, and ATP by HF-EPR and ENDOR spectroscopies. Multifrequency EPR analysis of [^{14}N]- and [^{15}N]-NH_2Y_{730}• in H_2O and D_2O allowed for accurate simulations of experimental spectra and revealed an unusually low g_x value of 2.0052, suggesting the importance of a local H-bonding environment.[35] Analysis of ND_2Y_{730}• using HF [^{2}H]-ENDOR spectroscopy (Figure 10), combined with structural information[24] and DFT calculations, allowed assignment of exchangeable protons in the immediate vicinity of the NH_2Y_{730}•.[21] These studies revealed strong intramolecular H bonds from the NH_2 group, two moderate H-bonding interactions (presumably with the adjacent pathway residues, Y_{731} and C_{439}), and a weaker interaction likely associated with an ordered water molecule. These results support a co-linear PCET mechanism within α2 by demonstrating a structured H-bonding network in the active $\alpha 2\beta 2$ complex.[21]

Mapping the Thermodynamic Landscape of the PCET Pathway

A Barrier to the RT Pathway: NO_2Y or F_nY. UAAs incorporated into RNR alter the thermodynamics from 260 mV easier to oxidize (DOPA) to 190 mV harder to oxidize (NO_2Y) than Y based on E_p measurements near physiological pH (Table 1). When the Y at position 356, 731, or 730 is replaced with NO_2Y, the resulting mutant is inactive, indicating that NO_2Y cannot be oxidized by other pathway radicals and hence cannot support RT. A series of F_nYs (**4**–**8**, Figure 4a, Table 1) incorporated at position 356 of β2 by EPL provided access to E_ps that varied from −50 to +250 mV relative to Y in the pH 6–9 range in which RNR is active (Figure 11).[18] pH rate profiles of these mutants demonstrated that their activities fell into three regimes based on the difference in E_p (ΔE_ps) between the F_nY (or F_nY^-)/F_nY• and Y/Y• couples. $Y_{356}F_nY$-β2s had activities resembling wt-β2 at ΔE_ps < 80 mV, whereas they were inactive at ΔE_ps > 200 mV, consistent with the results of NO_2Y mutants. In the range from 80–200 mV, $Y_{356}F_nY$-β2s exhibited measurable activities that decreased with increasing ΔE_p.[16]

A Sink in the RT Pathway: DOPA or NH_2Y. Substitution of pathway residues by DOPA or NH_2Y (**2** and **3**, Figure 4a) has allowed us to explore the consequence of lowering the potential at positions on the pathway by 260 and 190 mV, respectively (Table 1). As noted above, Y_{356}DOPA-β2 is catalytically inactive, presumably due to the inability of $DOPA_{356}$• to oxidize Y_{731}. We expected that NH_2Y-RNRs would also be inactive; however, these three mutants possessed 3–12% of the activity of their corresponding wt subunits (please see Footnote 1$^{\perp}$).[17,24] The combination of kinetically competent NH_2Y• formation and catalytic dNDP formation in NH_2Y-RNRs presents an opportunity to measure solvent isotope effects at individual steps in the RT pathway and during NDP reduction, providing insight on mechanistic

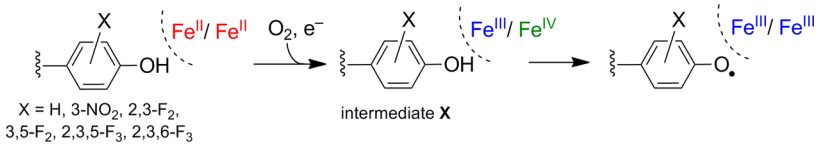

FIGURE 12. Assembly of the diferric-Y_{122}• (or NO_2Y_{122}• or F_nY_{122}•) cofactor from diferrous-β2, O_2, and reductant.

SCHEME 1. Kinetic Model for Radical Initiation in the Reaction of $Y_{122}NO_2Y$-β2 with wt-α2, S, and E[29]

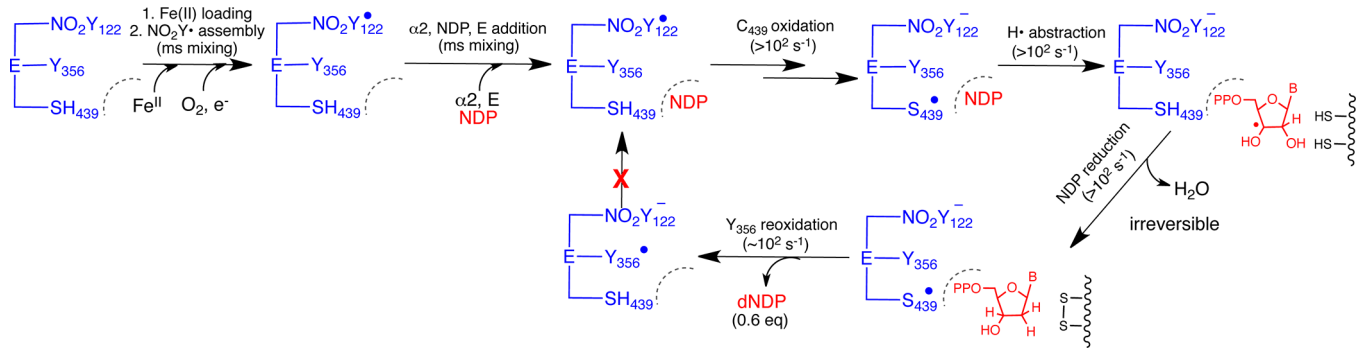

details that are kinetically masked in the wt enzyme.[14] In summary, activity measurements of RNRs containing UAAs indicate that the thermodynamics of RT can be modulated by $\leq \pm 200$ mV relative to the native pathway at positions 356, 731, and 730 while retaining some enzymatic activity.

Increasing the Driving Force of RT at Position 122: NO_2Y and F_nYs. In an effort to characterize the native Y• intermediates, we replaced Y_{122} with NO_2Y and F_nYs (**1** and **4**–**7**, Figure 4a). We anticipated the ability to generate radicals of NO_2Y and F_nYs at this position given the unique mechanism of diferric-Y_{122}• assembly in the wt enzyme, which utilizes a strongly oxidizing Fe^{3+}/Fe^{4+} intermediate ("X", Figure 12).[7] A three-syringe, double-mixing apparatus was employed for these experiments in which Fe^{II}-loaded $Y_{122}NO_2Y$-β2 was rapidly mixed with O_2-saturated buffer to generate NO_2Y_{122}• (1.2 eq/β2, $t_{1/2}$ ~40 s at 25 °C) on the first syringe drive, followed immediately by reaction of this short-lived NO_2Y_{122}• with wt-α2, S, and E on the second syringe drive (Scheme 1, step 1).[29] The reaction was monitored by SF, RFQ-EPR, RFQ-PELDOR, and RCQ methods (Figure 5), and the results are summarized in Scheme 1.[29] After assembly of the active cofactor, NO_2Y_{122}• is rapidly reduced (>100 s^{-1}) in the first step of RT to generate the phenolate ($NO_2Y_{122}^-$) rather than the anticipated phenol, indicating an uncoupling of PT from ET. All subsequent steps, including formation of dCDP and a new Y•(s), occurred with similar rate constants (>100 s^{-1}). The ability to detect dCDP and new Y• formation at rate constants 10- to 50-fold faster than the wt k_{cat} indicated that disruption of the PT/ET coupling in the first step bypassed the conformational change that is rate-determining in the wt enzyme. Only 0.6 equiv dCDP/β2 and 0.6 equiv Y•/β2 were generated in this process, indicating that the mutant enzyme (1.2 NO_2Y_{122}•/β2) could perform only a single turnover with half-sites reactivity, presumably due to inability to reoxidize the $NO_2Y_{122}^-$ to NO_2Y_{122}• during reverse RT.

The results of additional studies of NO_2Y-containing β2s with either additional mutations of pathway residues (Y-to-F or Y-to-3,5-F_2Y) or globally labeled β-[^{2}H]-Ys, in conjunction with HF EPR and PELDOR spectroscopies, indicated that the observed Y• is generated during reverse RT and exists as an equilibrium of radicals at positions 356, 731, and 730 in ~10:1:1 ratio.[12,29] These findings provide the basis for the relative positioning of Y_{356}, Y_{731}, and Y_{730} in the proposed thermodynamic landscape of the RT pathway (Figure 3b).[12]

To explore reactivity in the ~200 mV regime separating NO_2Y and Y, a series of F_nYs (**4**–**7**, Figure 4a) was incorporated in place of Y_{122}. Assuming that $Y_{122}F_nY$-β2s experience a pK_a perturbation similar to that of NO_2Y_{122} (>2.5 units),[28] all F_nYs would remain protonated at pH 7.6 and would vary from 50 mV easier to 100 mV harder to oxidize than Y (Figures 3b and 11).[18] Using an evolved, polyspecific F_nY-RS, four $Y_{122}F_nY$-β2s were isolated, and the assembly and stability of their F_nY_{122}•s were spectroscopically characterized.[13,14] Their EPR spectra feature hyperfine couplings of the radical to the fluorine nuclei, giving rise to sharp low- and high-field features that facilitate spectral deconvolution of F_nY_{122}•s from pathway Y•s (Figure 13a).[13] All $Y_{122}F_nY$-β2s are active in the steady-state with 10–100% the activity of wt-β2.[14] When the

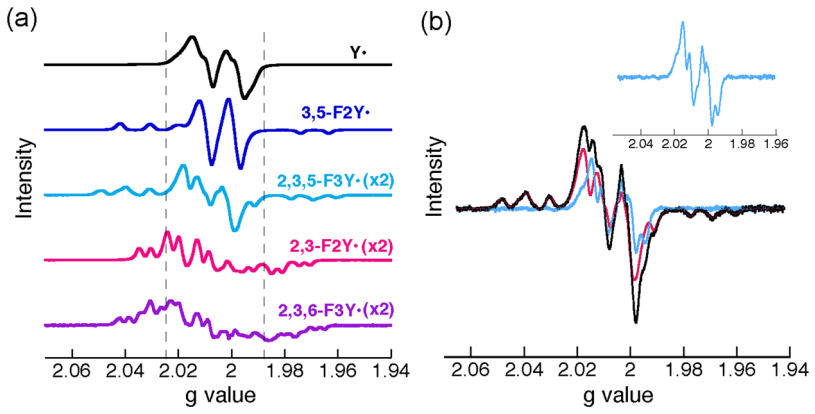

FIGURE 13. (a) X-band EPR spectra (77 K) for *E. coli* Y_{122}• and F_nY_{122}•s normalized for radical concentration. Dashed lines highlight the increased spectral width of the F_nY_{122}•s.[13,14] (b) EPR spectrum of the reaction of Y_{122}(2,3,5)F_3Y-β2, wt-α2, CDP, and ATP quenched at 25 s. The reaction spectrum (black) is a composite of two species: 2,3,5-F_3Y_{122}• (pink) and a new radical (blue, magnified in inset), assigned as Y_{356}•. Adapted (in part) with permission from ref 13. Copyright 2011 American Chemical Society.

driving force of RT is raised relative to Y, reaction of $Y_{122}F_nY$-β2s with wt-α2 (or Y_{731}F-α2), S, and E resulted in loss of F_nY_{122}• concomitant with the generation of a new radical, hypothesized to be Y_{356}• generated during forward RT (Figure 13b).[13,14] The kinetics of new radical formation and dCDP production have been studied for the reaction of Y_{122}(2,3,5)F_3Y-β2 with wt-α2, CDP, and ATP, and indicate that Y_{356}• formation is kinetically competent relative to dCDP formation.[14]

Finally, the ability to monitor oxidation of Y_{356} by NO_2Y_{122}• or F_nY_{122}•s has allowed us to address the function of W_{48} (Figure 3a).[2,7] This residue has been shown to participate during in vitro cofactor assembly, but its role in long-range RT has not been established. Preliminary studies of the reactivity of $Y_{122}NO_2Y/Y_{356}$F-β2 or Y_{122}(2,3,5)F_3Y/Y_{356}F-β2 double mutants provided no evidence for the formation of a discrete W_{48}•/W_{48}•+ intermediate during in RT, although it is possible that W_{48} plays an important role in conformational gating.[13,14,29]

From the studies conducted to date, a thermodynamic landscape for the RT pathway is emerging (Figure 3b). This model indicates that position 122 is the pathway minimum; however, detection of Y_{356}• in the reaction with Y_{122}(2,3,5)F_3Y-β2 as a radical initiator suggests that the thermodynamic difference between position 122 and 356 is small and that the stability of Y_{122}• may be kinetic in origin. W_{48} is colored in gray, as we currently have no evidence in support of its participation as a discrete radical intermediate. The three transiently oxidized Ys are harder to oxidize than Y_{122}, with Y_{731} and Y_{730} 50−100 mV harder to oxidize than Y_{356} and roughly isoenergetic with one another.[12] Finally, C_{439} is placed at a reduction potential quite similar to or slightly elevated above the 730/731 dyad based on the solution reduction potential of glutathione radical at neutral pH.[36] In our model, the forward RT pathway is thus uphill, and C_{439} oxidation is driven by the rapid, irreversible loss of water in the second step of nucleotide reduction (Figure 2),[1,3] and the reverse RT pathway is downhill and rapid.

Conclusions

This Account summarizes the results of recent mechanistic studies on mutant *E. coli* class Ia RNRs containing unnatural Y analogues at the proposed sites of stable and transient Y• formation on the RT pathway. Specifically, the results obtained from unnatural DOPA-, NH_2Y-, NO_2Y-, and F_nYs-RNRs and light-initiated photo-RNRs were used to establish (1) that there exists a specific pathway containing a minimum of four Ys involved in long-range RT over 35 Å across a compact, globular $\alpha2\beta2$ resembling Uhlin and Eklund's docking model; (2) that RT occurs by orthogonal and co-linear PCET transfers in the β2 and α2 subunits, respectively; (3) that the overall thermodynamics of RT are only slightly uphill in the forward direction, with several of the intervening steps being nearly isoenergetic; (4) that the individual RT steps and the chemistry of nucleotide reduction are fast ($\sim10^5$ and >100 s^{-1}, respectively), despite being kinetically masked by several conformational changes (10−100 s^{-1}) that occur when nucleotides bind to $\alpha2\beta2$; and (5) that the rate-limiting conformational changes likely target the RT pathway and its tightly coupled proton and electron transfers.

We would like to thank the many researchers with whom we have fruitfully collaborated on this project, and we regret that space constraints have prevented us from recognizing each of

them and their unique contributions in this Account. We thank Arturo Pizano for assistance with Figure 9. This work was supported by the NIH Grants GM47274 (to D.G.N.) and GM29595 (to J.S.).

ABBREVIATIONS

α2, RNR large subunit; β2, RNR small subunit; E, effector; E_p, peak potential; ET, electron transfer; HF, high-field; N_3UDP, 2′-azido-2′-deoxyuridine 5′-diphosphate; PCET, proton-coupled electron transfer; PO, photooxidant; PT, proton transfer; RT, radical transfer; S•, cysteine radical; S, substrate; UAA, unnatural amino acid; wt, wild-type; Y•, tyrosyl radical;

BIOGRAPHICAL INFORMATION

Ellen C. Minnihan conducted graduate research in the Stubbe lab and earned her Ph.D. in Chemistry from MIT in 2012.

Daniel G. Nocera is the Patterson Rockwood Professor of Energy at Harvard University. His research focuses on the study of PCET as it pertains to the biology of nucleotide metabolism and energy conversion.

JoAnne Stubbe, the Novartis Professor of Chemistry and Professor of Biology at MIT, has dedicated her career to the study of the mechanisms of ribonucleotide reductases and other enzymatic systems.

FOOTNOTES

*To whom correspondence should be addressed. E-mail: nocera@fas.harvard.edu (D.G.N.); stubbe@mit.edu (J.S.).

The authors declare no competing financial interest.

⊥Footnote 1: This result was unexpected, as the ΔE_p between Y and NH_2Y is near the 200 mV threshold observed to shut down RT. However, the E_ps reported herein (Table 1)[15,17−19] have been measured by various methods by different researchers, and thus, significant error could exist in our calculated ΔE_ps. We are collaborating with the Koppenol lab to remeasure the potentials of these UAAs to obtain a single set of reliable values. Further error arises from the fact that E_p values are sensitive to the reaction conditions under which they were measured, and thus the observed E_ps may differ significantly from true reduction potentials ($E°$s).

REFERENCES

1 Stubbe, J.; van der Donk, W. A. Protein radicals in enzyme catalysis. *Chem. Rev.* **1998**, *98*, 705–762 and references therein.

2 Uhlin, U.; Eklund, H. Structure of ribonucleotide reductase protein R1. *Nature* **1994**, *370*, 533–539.

3 Licht, S.; Stubbe, J. Mechanistic investigations of ribonucleotide reductases. *Compr. Nat. Prod. Chem.* **1999**, *5*, 163–203 and references therein.

4 Climent, I.; Sjöberg, B. M.; Huang, C. Y. Carboxyl-terminal peptides as probes for *Escherichia coli* ribonucleotide reductase subunit interaction: kinetic analysis of inhibition studies. *Biochemistry* **1991**, *30*, 5164–5171.

5 Ge, J.; Yu, G.; Ator, M. A.; Stubbe, J. Pre-steady-state and steady-state kinetic analysis of *E. coli* class I ribonucleotide reductase. *Biochemistry* **2003**, *42*, 10071–10083.

6 Climent, I.; Sjöberg, B. M.; Huang, C. Y. Site-directed mutagenesis and deletion of the carboxyl terminus of *Escherichia coli* ribonucleotide reductase protein R2-effects on catalytic activity and subunit interaction. *Biochemistry* **1992**, *31*, 4801–4807.

7 Stubbe, J.; Nocera, D. G.; Yee, C. S.; Chang, M. C. Y. Radical initiation in the class I ribonucleotide reductase: long-range proton-coupled electron transfer? *Chem. Rev.* **2003**, *103*, 2167–2201 and references therein.

8 Cukier, R. I.; Nocera, D. G. Proton-coupled electron transfer. *Annu. Rev. Phys. Chem.* **1998**, *49*, 337–369.

9 Mayer, J. M. Proton-coupled electron transfer: a reaction chemist's view. *Annu. Rev. Phys. Chem.* **2004**, *55*, 363–390.

10 Reece, S. Y.; Hodgkiss, J. M.; Stubbe, J.; Nocera, D. G. Proton-coupled electron transfer: the mechanistic underpinning for radical transport and catalysis in biology. *Philos. Trans. R. Soc. London, Ser. B* **2006**, *361*, 1351–1364 and references therein.

11 Reece, S. Y.; Nocera, D. G. Proton-coupled electron transfer in biology: results from synergistic studies in natural and model systems. *Annu. Rev. Biochem.* **2009**, *78*, 673–699 and references therein.

12 Yokoyama, K.; Smith, A. A.; Corzilius, B.; Griffin, R. G.; Stubbe, J. Equilibration of tyrosyl radicals (Y356•, Y731•, Y730•) in the radical propagation pathway of the *Escherichia coli* class Ia ribonucleotide reductase. *J. Am. Chem. Soc.* **2011**, *133*, 18420–18432.

13 Minnihan, E. C.; Young, D. D.; Schultz, P. G.; Stubbe, J. Incorporation of fluorotyrosines into ribonucleotide reductase using an evolved, polyspecific aminoacyl-tRNA synthetase. *J. Am. Chem. Soc.* **2011**, *133*, 15942–15945.

14 Minnihan, E. C. Ph.D. Thesis, Massachusetts Institute of Technology, 2012.

15 Yee, C. S.; Seyedsayamdost, M. R.; Chang, M. C. Y.; Nocera, D. G.; Stubbe, J. Generation of the R2 subunit of ribonucleotide reductase by intein chemistry: insertion of 3-nitrotyrosine at residue 356 as a probe of the radical initiation process. *Biochemistry* **2003**, *42*, 14541–14552.

16 Seyedsayamdost, M. R.; Yee, C. S.; Reece, S. Y.; Nocera, D. G.; Stubbe, J. pH rate profiles of F_nY_{356}-R2s (n = 2, 3, 4) in *Escherichia coli* ribonucleotide reductase: evidence that Y_{356} is a redox-active amino acid along the radical propagation pathway. *J. Am. Chem. Soc.* **2006**, *128*, 1562–1568.

17 Seyedsayamdost, M. R.; Xie, J.; Chan, C. T.; Schultz, P. G.; Stubbe, J. Site-specific insertion of 3-aminotyrosine into subunit α2 of *E. coli* ribonucleotide reductase: direct evidence for involvement of Y730 and Y731 in radical propagation. *J. Am. Chem. Soc.* **2007**, *129*, 15060–15071.

18 Seyedsayamdost, M. R.; Reece, S. Y.; Nocera, D. G.; Stubbe, J. Mono-, di-, tri-, and tetra-substituted fluorotyrosines: new probes for enzymes that use tyrosyl radicals in catalysis. *J. Am. Chem. Soc.* **2006**, *128*, 1569–1579.

19 Seyedsayamdost, M. R.; Stubbe, J. Site-specific replacement of Y_{356} with 3,4-dihydroxyphenylalanine in the β2 subunit of *E. coli* ribonucleotide reductase. *J. Am. Chem. Soc.* **2006**, *128*, 2522–2523.

20 Bennati, M.; Robblee, J. H.; Mugnaini, V.; Stubbe, J.; Freed, J. H.; Borbat, P. EPR distance measurements support a model for long-range radical initiation in *E. coli* ribonucleotide reductase. *J. Am. Chem. Soc.* **2005**, *127*, 15014–15015.

21 Argirevic, T.; Riplinger, C.; Stubbe, J.; Neese, F.; Bennati, M. ENDOR spectroscopy and DFT calculations: Evidence for the hydrogen-bond network within α2 in the PCET of *E. coli* ribonucleotide reductase. *J. Am. Chem. Soc.* **2012**, *134*, 17661–17670.

22 Gerfen, G. J.; Bellew, B. F.; Un, S.; Joseph M. Bollinger, J.; Stubbe, J.; Griffin, R. G.; Singel, D. J. High-frequency (139.5 GHz) EPR spectroscopy of the tyrosyl radical in *Escherichia coli* ribonucleotide reductase. *J. Am. Chem. Soc.* **1993**, *115*, 6420–6421.

23 Seyedsayamdost, M. R.; Chan, C. T.; Mugnaini, V.; Stubbe, J.; Bennati, M. PELDOR spectroscopy with DOPA-β2 and NH_2Y-α2s: distance measurements between residues involved in the radical propagation pathway of *E. coli* ribonucleotide reductase. *J. Am. Chem. Soc.* **2007**, *129*, 15748–15749.

24 Minnihan, E. C.; Seyedsayamdost, M. R.; Uhlin, U.; Stubbe, J. Kinetics of radical intermediate formation and deoxynucleotide production in 3-aminotyrosine-substituted *Escherichia coli* ribonucleotide reductases. *J. Am. Chem. Soc.* **2011**, *133*, 9430–9440.

25 Minnihan, E. C.; Seyedsayamdost, M. R.; Stubbe, J. Use of 3-aminotyrosine to examine the pathway dependence of radical propagation in *Escherichia coli* ribonucleotide reductase. *Biochemistry* **2009**, *48*, 12125–12132.

26 Minnihan, E. C.; Ando, N.; Brignole, E. J.; Olshansky, L.; Chittuluru, J.; Asturias, F.; Drennan, C. L.; Nocera, D. G.; Stubbe, J. Generation of a stable, aminotyrosyl radical-induced $\alpha2\beta2$ complex of *E. coli* class Ia RNR. *Proc. Natl. Acad. Sci. U.S.A.* **2013**, *110*, 3835–3840.

27 Hassan, A. Q.; Olshansky, L.; Yokoyama, K.; Nocera, D. G.; Stubbe, J. In revision.

28 Yokoyama, K.; Uhlin, U.; Stubbe, J. Site-specific incorporation of 3-nitrotyrosine as a probe of pK_a perturbation of redox-active tyrosines in ribonucleotide reductase. *J. Am. Chem. Soc.* **2010**, *132*, 8385–8397.

29 Yokoyama, K.; Uhlin, U.; Stubbe, J. A hot oxidant, 3-NO_2Y_{122} radical, unmasks conformational gating in ribonucleotide reductase. *J. Am. Chem. Soc.* **2010**, *132*, 15368–15379.

30 Yee, C. S.; Chang, M. C. Y.; Ge, J.; Nocera, D. G.; Stubbe, J. 2,3-difluorotyrosine at position 356 of ribonucleotide reductase R2: A probe of long-range proton-coupled electron transfer. *J. Am. Chem. Soc.* **2003**, *125*, 10506–10507.

31 Wörsdörfer, B.; Conner, D. A.; Yokoyama, K.; Seyedsayamdost, M.; Jiang, W.; Stubbe, J.; Bollinger, J. M.; Krebs, C. Function of the diiron cluster in *Escherichia coli* class Ia ribonucleotide reductase in proton-coupled electron transfer. *J. Am. Chem. Soc.* **2013**, DOI: 10.1021/ja401342s.

32 Reece, S. Y.; Seyedsayamdost, M. R.; Stubbe, J.; Nocera, D. G. Photoactive peptides for light-initiated tyrosyl radical generation and transport into ribonucleotide reductase. *J. Am. Chem. Soc.* **2007**, *129*, 8500–8509.

33 Holder, P. G.; Pizano, A. A.; Anderson, B. L.; Stubbe, J.; Nocera, D. G. Deciphering radical transport in the large subunit of class I ribonucleotide reductase. *J. Am. Chem. Soc.* **2012**, *134*, 1172–1180.

34 Pizano, A. A.; Lutterman, D. A.; Holder, P. G.; Teets, T. S.; Stubbe, J.; Nocera, D. G. Photoribonucleotide reductase β2 by selective cysteine labeling with a radical phototrigger. *Proc. Natl. Acad. Sci. U.S.A.* **2011**, *109*, 39–43.

35 Seyedsayamdost, M. R.; Argirevic, T.; Minnihan, E. C.; Stubbe, J.; Bennati, M. Structural examination of the transient 3-aminotyrosyl radical on the PCET pathway of *E. coli* ribonucleotide reductase by multifrequency EPR spectroscopy. *J. Am. Chem. Soc.* **2009**, *131*, 15729–15738.

36 Madej, E.; Wardman, P. The oxidizing power of the glutathione thiyl radical as measured by its electrode potential at physiological pH. *Arch. Biochem. Biophys.* **2007**, *462*, 94–102.